Journal of Industrial and Engineering Chemistry 150 (2025) 719–733

Contents lists available at ScienceDirect

Journal of Industrial and Engineering Chemistry

journal homepage: www.elsevier.com/locate/jiec

Full Length Article

Repurposing expired Remdesivir as a sustainable anti-corrosion agent for plain steel in HCl medium: Insights from electrochemical and molecular dynamics studies

Ismat H. Ali [a], Ruhollah Sharifi [b], Ali Asghar Javidparvar [c,*], Simeon C. Nwanonenyi [d], Emeka E. Oguzie [d], Theodore A. Manfo [e,*]

[a] Chemistry Department, King Khalid University, Abha, Saudi Arabia
[b] Department of Materials Science and Engineering, Sharif University of Technology, Tehran, Iran
[c] School of Metallurgy and Materials Engineering, College of Engineering, University of Tehran, P.O. Box 11155-4563, Tehran, Iran
[d] Africa Centre of Excellence in Future Energies and Electrochemical Systems, Federal University of Technology, PMB 1529, Owerri, Imo State, Nigeria
[e] Department of Electrical Engineering and Energy Technology, School of Technology and Innovations, University of Vaasa, Wolffintie 32, 65200 Vaasa, Finland

A B S T R A C T

The COVID-19 pandemic has led to a surplus of expired pharmaceuticals, such as Remdesivir, posing environmental challenges. This study innovatively repurposes expired Remdesivir as a highly effective sustainable anti-corrosion agent for St12 mild steel in a 1 M HCl environment. Experimental and computational analyses reveal that Remdesivir's molecular structure, featuring nitrogen and oxygen heteroatoms and multiple benzene rings, enables strong chemisorption on the steel surface, forming a dense protective layer. At an optimal concentration of 1000 ppm, Remdesivir achieves over 97 % corrosion inhibition efficiency. Molecular dynamics simulations confirm a spontaneous and stable interaction, with binding energies of −205.69 kcal/mol (gaseous phase) and −144.314 kcal/mol (solvated phase), highlighting its durable protective capabilities. This work not only offers an eco-friendly solution for managing expired drugs but also demonstrates their potential to enhance the longevity of metallic structures in corrosive environments, combining environmental sustainability with industrial applicability.

Introduction

After the discovery of effective vaccines against COVID-19 and the subsequent reduction in disease-related deaths in 2021, the environmental impact of the massive quantities of medical waste generated, including expired drugs used to treat the illness, has become a growing concern [1–3]. Remdesivir, an antiviral drug initially developed to treat Ebola virus infections, has shown efficacy in reducing the severity of symptoms and accelerating recovery in hospitalized COVID-19 patients [2,3]. As a nucleotide analog, Remdesivir mimics RNA building blocks, interfering with viral replication by causing errors in the RNA strand, thereby preventing the virus from producing more copies of itself [4,5]. Clinical trials have demonstrated its ability to shorten recovery time and reduce the risk of severe disease progression in hospitalized patients, although it is not a cure for COVID-19 [6,7]. However, like all medications, Remdesivir has a limited shelf life and can expire if not used within a specific timeframe [8–10].

Improper disposal of expired drugs, such as Remdesivir, can lead to significant environmental risks. These medications may leach into water sources, contaminate soil, and harm wildlife [11,12]. Moreover, improper disposal can contribute to the development of antibiotic-resistant bacteria and other harmful pathogens, exacerbating public health challenges [13,14]. In the context of COVID-19 treatments, the large volume of medications used—and potentially expired—further amplifies these environmental concerns. Hospitals and healthcare facilities, often under immense pressure to treat patients, may lack the necessary resources or protocols to ensure proper disposal of expired medications. To mitigate these risks, it is essential for healthcare facilities and pharmaceutical companies to adopt and enforce effective waste management practices [15].

Expired drugs have been demonstrated to be effective corrosion inhibitors for metals and alloys [16]. The chemical structure of Remdesivir, featuring various heteroatoms, multiple bonds, and benzene rings, makes it a promising candidate for use as a sustainable anti-corrosion agent (SAA) for metals immersed in corrosive media [17,18]. SAAs are substances that, when added to a corrosive environment, can slow down or prevent metal deterioration [19,20]. The heteroatoms in Remdesivir enable the formation of coordination complexes with Fe ions, effectively inhibiting corrosion by creating a dense protective layer on the metal surface [21,22]. Moreover, the multiple bonds and benzene rings in

* Corresponding authors.
E-mail addresses: Javidparvar@ut.ac.ir (A.A. Javidparvar), Theodore.azemtsop.manfo@uwasa.fi (T.A. Manfo).

https://doi.org/10.1016/j.jiec.2025.03.036
Received 25 January 2025; Received in revised form 7 March 2025; Accepted 17 March 2025
Available online 21 March 2025

Remdesivir's structure facilitate electron delocalization, further enhancing its corrosion inhibition performance [23,24]. Additionally, Remdesivir's biodegradability offers an ecological advantage. Unlike traditional anti-corrosion agents, which may pose environmental risks, expired Remdesivir as a green SAA has the potential to break down into harmless byproducts over time, reducing its ecological footprint [25,26]. In fact, the COVID-19 pandemic led to the overproduction of Remdesivir, and following the development of effective vaccines, a significant surplus of this drug has remained unused, posing environmental challenges. The innovative repurposing of expired Remdesivir as a sustainable anti-corrosion agent (SAA) addresses these environmental concerns while providing a cost-effective solution. This study demonstrates the novel application of expired Remdesivir, which combines the drug's unique chemical structure with eco-friendly and economically beneficial practices. By repurposing the surplus of this drug, we not only mitigate environmental risks but also find a valuable use for otherwise wasted pharmaceuticals.

To the best of our knowledge, the investigation into using expired drugs as corrosion inhibitors was initiated by R. S. Abdel Hameed in 2009, when he employed expired Ranitidine (active substance: ranitidine hydrochloride) as a corrosion inhibitor for aluminum in hydrochloric acid solutions [27]. He and his colleagues also conducted a study on the green synthesis, characterization, and inhibitory properties of silver nanoparticles (AgNPs) using expired Baclofen drugs collected from Hail City, Saudi Arabia. The study found that adding polyvinyl alcohol (PVA) and expired pharmaceuticals to the nanoparticles significantly increased the corrosion inhibition of steel. The results demonstrated that higher concentrations of nanoparticles, expired drugs, and increased reaction temperatures improved corrosion inhibition, with the inhibition following the Langmuir Isotherm [28].

Metwally Abdallah and his team studied the use of expired azithromycin (AZM) and roxithromycin (RXM) as corrosion inhibitors for mild steel in H_2SO_4, finding that increased drug concentrations and lower temperatures improved inhibition efficiency through adsorption on the steel surface. RXM showed greater inhibition efficiency than AZM due to its higher molecular weight and more electron-donating groups [29]. They also studied the effects of expired antibacterial drugs, amoxicillin (Amo) and cefuroxime (Cef), on the corrosion behavior of Sabic iron in 1.0 M HCl solution. They found that increasing the concentration of these drugs enhanced the inhibition efficiency, with the inhibition process following the Langmuir isotherm. The study showed that these expired drugs serve as efficient mixed-type inhibitors, forming a protective film on the iron surface [30]. Al-Gorair et al. [31] investigated the inhibition of carbon steel corrosion in hydrochloric acid using Salbutamol extracted from expired Farcolin drugs. Their study demonstrated that the effectiveness of Salbutamol as a corrosion inhibitor improved with increased dosage, polarization resistance, and lower corrosion current density, following the Langmuir isotherm. The study showed significant potential for recycling expired drugs to create efficient corrosion inhibitors. Aboubakr Saleh et al. [32] investigated the inhibition of plain steel corrosion in hydrochloric acid using a Schiff base inhibitor, DMAB. They found that the corrosion rate decreased with higher concentrations of DMAB, reaching an inhibition efficacy of 97.7 % at 5.0 mM and 298 K, following the Langmuir adsorption isotherm. The study combined experimental techniques and theoretical quantum computations to confirm the effectiveness of DMAB as a corrosion inhibitor. In addition, a recent study examined the use of expired lactulose drugs as eco-friendly corrosion inhibitors for steel alloys in acidic environments. The research assessed the effectiveness of lactulose using electrochemical and gravimetric methods, finding that corrosion inhibition increased with higher drug concentration and lower pH. The results demonstrated that expired lactulose acts as a mixed-type inhibitor, following the Langmuir adsorption isotherm [33]. Another study evaluated the anticorrosion potency of expired antifungal drugs, bifonazole (BIF) and terconazole (TER), for X65 carbon steel in 1.0 M HCl solution using practical and computational measurements. Results showed increased anticorrosive efficacy with higher concentrations of BIF and TER, with adsorption following the Langmuir isotherm. Both drugs acted as mixed inhibitors, improving corrosion resistance and shifting pitting potential to positive values, as confirmed by impedance and polarization methods [34].

Deyab et al. [35] utilized favipiravir, another widely used drug for COVID-19 treatment, as a sustainable anti-corrosion agent (SAA) for an aluminum–silicon alloy immersed in 1 M HCl. Their results demonstrated that this biocompatible and eco-friendly agent acted as a mixed-type inhibitor with a predominant cathodic effect. At a concentration of 100 ppm, the agent achieved a remarkable corrosion inhibition efficiency of 96 %. Quantum chemical calculations revealed a high binding energy of 212 kcal/mol, indicating a strong tendency for adsorption on the Al-Si alloy surface. In another study, Kellenberger et al. [36] explored the use of expired Midazolam, a drug used during the pandemic, as a green anti-corrosion agent for copper coupons in a 0.1 M nitric acid electrolyte. The mixed-type inhibitor exhibited an inhibition efficiency of approximately 93 % at a concentration of 0.1 mM and was found to follow the Langmuir adsorption isotherm. Additionally, Peng et al. [37] investigated the use of an ethanolic extract of expired Yan-ReQing Granules, a traditional Chinese patent medicine widely used during the COVID-19 epidemic in China, as an anti-corrosion agent for Q235 steel in 0.1 M HCl. The extract demonstrated an exceptional corrosion inhibition efficiency of 99 % and was classified as a mixed-type inhibitor.

In this study, expired Remdesivir drug (ERD) was explored as a sustainable anti-corrosion agent (SAA) for St12 steel immersed in 1.0 M HCl, addressing both environmental and economic concerns. The corrosion inhibition potential of ERD was evaluated through electrochemical tests and supported by theoretical studies, highlighting its effectiveness in protecting the electrode in an acidic environment.

Materials and methods

Materials

The St12 steel used in this study had the following weight percentages: Mn: 1.12, Cr: 0.71, Ni: 1.74, Si: 1.12, Mo: 1.01, P: 1.22, Ti: $<$0.01, and Fe as the remainder. Steel plates measuring 5 cm $\times$ 3 cm $\times$ 0.2 cm were polished using 600, 800, and 1200-grit sandpaper. They were then cleaned twice with a water/acetone mixture and dried. Remdesivir with a purity of 98.3 %, which had expired approximately 2 years prior, was obtained from CoQua Lab (Turin, Italy). St12 mild steel was selected as the substrate due to its widespread industrial applications and susceptibility to corrosion in acidic environments. The corrosion medium was chosen as 1 M HCl because hydrochloric acid is commonly used in industrial processes such as pickling, metal cleaning, and acid descaling, making it a relevant and well-established medium for evaluating corrosion inhibitors. All experiments were conducted at ambient temperature ($\sim$25 °C) to simulate standard operating conditions where corrosion inhibitors are typically applied in real-world industrial settings. Since Remdesivir has limited solubility in water, a minimal amount of ethanol was used as a co-solvent to ensure complete dissolution and uniform dispersion in the 1 M HCl solution. This approach prevents precipitation and ensures effective interaction between the inhibitor molecules and the metal surface. All abbreviations used in this study are listed in Table S1.

Methods

Structural analysis and surface studies

FT-IR and UV–Vis spectroscopy were employed to identify the functional groups of the inhibitor. UV–Vis data were collected using a Hitachi U-3010 UV–Vis spectrophotometer, while FT-IR spectra were obtained using a Thermo Scientific Nicolet 6700 instrument with a wavenumber range of 400–4000 cm^{-1}. XPS analysis was conducted

using a Kratos Axis Ultra Imaging X-ray photoelectron spectrometer equipped with an Al Kα source at a pressure of 10^{-9} mbar. EDS and elemental mapping studies were performed using a LEO 1455VP instrument. FE-SEM micrographs were acquired with a JEM-2100F device. Additionally, atomic force microscopy (AFM) measurements were carried out using a NANONICS Academia model instrument, and contact angle analysis was performed using an OCA plus apparatus.

Electrochemical measurements

Electrochemical techniques were applied to the St12 coupons, which had an exposed surface area of 1 cm^2. A three-electrode cell setup was used, where the prepared St12 plates served as the WE, a SCE acted as the RE, and a platinum electrode was employed as the CE. An Ivium potentiostat was used to conduct the measurements. For the EIS analysis, a frequency range of 10 kHz to 100 mHz and a signal amplitude perturbation of 10 mV were selected. PDP analysis was conducted at a scan rate of 1 mV/s within a range of ± 250 mV vs. the OCP. All electrochemical measurements were performed under stagnant conditions.

Theoretical computation section

The software used for theoretical computation was Material Studio from BIOVIA and techniques employed for the molecular computation were QCC and MDS. The computational module tools used for QCC and MDS include; sketch tool, 3D atomistic document, $DMol^3$, Adsorption locator, Forcite, etc.

Qccs

The electronic structure of Remdesivir molecule was drawn in atomistic document with sketch tool while geometrical optimization was done with $DMol^3$ tool in order to evaluate some chemical reactivities associated with molecule. The correlation exchange functions of GGA, DND, Perdew-Burke-Ernzerh (PBE), unrestricted spin, and 3.5 basis set were the useful parameters for the optimization.

MDS

The electronic structure of the metal substrate (Fe) was imported and placed in an atomistic model. The Forcite tool was used to optimize the metal surface, which was then cleaved along the (110) plane. An enlarged supercell with dimensions of 12 × 10 was created within the simulation box, providing a large surface area to accommodate interactions between the inhibitive systems, the metal surface, and other corrosive agents present in the electrolytic environment. Additionally, the cleaved metal surface was constructed into a crystal structure with a position of 1.00 Å and a slab crystal thickness of 25 Å. The constituents of the electrolytic system, including $500H_2O$ molecules, $10Cl^-$ ions, and $5H_3O^+$ ions, were packed onto the metal crystal surface using the Adsorption Locator tool within the simulation box. The Remdesivir molecule was then docked onto the metal crystal surface. Finally, the constituents of the simulation box were geometrically optimized and subjected to quench dynamics. The essential parameters used for optimization were as follows: algorithm (Smart), force (0.5 kcal/mol/Å), maximum iterations (1000), displacement (0.015 Å), energy (0.001 kcal/mol), and COMPASS forcefield. The quench dynamic parameters included: NVE ensemble, number of steps (5000), COMPASS forcefield, total simulation time (5.0 ps), temperature (298 K), quench steps (250), and time step (1 fs). Finally, the binding energy of adsorption (Eadsorption), which provides information on the interactive forces between the metal surface (110), the adsorbed inhibitor film, and the electrolytic constituents, was computed using Equation (1) as stated below [38]:

$$E_{\text{Binding energy}} = E_{\text{Total}} - (E_{\text{MEC}} + E_{\text{inhibitor molecule}}) \quad (1)$$

where $E_{\text{Binding energy}}$, E_{Total}, E_{MES}, $E_{\text{inhibitor molecule}}$ represents adsorption energy joining metal crystal surface and inhibitor species, total adsorption energy, energy of adsorption of metal and electrolytic constituents, and adsorption energy of inhibitor species.

Results and discussion

FTIR spectroscopy

The presence of chemical bonds in the ERD, as well as the influence of the drug's expiration on its chemical structure, was investigated using FTIR spectroscopy (Fig. 1). The chemical bonds corresponding to each absorption peak are reported in Table 1.

According to Fig. 1 and considering the negligible changes in the absorption peak positions in the FTIR spectra of the fresh and expired drugs, it can be concluded that the overall chemical structure of the drug does not show significant differences after expiration compared to the fresh drug. The lack of substantial changes in the chemical structure of drugs after their expiration date has been previously demonstrated in an investigation conducted by Pentagon and published by the FDA in 1985. According to the results of that study, 90 % of the therapeutic properties of expired drugs remain intact even after a long period of expiration [51,52]. Therefore, based on Table 1, the presence of C≡N, C-N, C=O, N–H, and C-O bonds in both fresh and expired drugs indicates that after two years of expiration, the multiple bonds and heteroatoms have not changed significantly, as has been previously demonstrated for other expired drugs[14,53]. However, the lower peak intensity of methyl and methylene groups, as well as the higher peak intensity of the hydroxyl bond at around 3320 cm^{-1} in the expired sample compared to the fresh drug, can be attributed to the hydrolysis process in the presence of moisture and sunlight [54,55].

Uv–vis analysis

UV–Vis spectroscopy is another useful technique for determining chemical bonds in the ERD structure. This analysis was also used to investigate the adsorption of SAA molecules on an immersed electrode in an acidic solution containing the inhibitor. Fig. 2 shows the UV–Vis spectra for the 1 M HCl solutions before and after soaking an St12 plate in them for 48 h.

In the UV–Vis spectra of both fresh and expired drugs, the observed peaks at around 265, 295, and 352 nm are attributed to C=C/C=N, C=O, and N≡C bonds, respectively[56–58]. The presence of all peaks related to the inhibitor's chemical structure in the UV–Vis spectrum of the electrode-containing solution indicates that the presence of the steel plate did not cause any significant changes in the chemical composition of the expired drug solution in hydrochloric acid. However, the decrease in peak intensities in the steel coupon-containing sample proves that

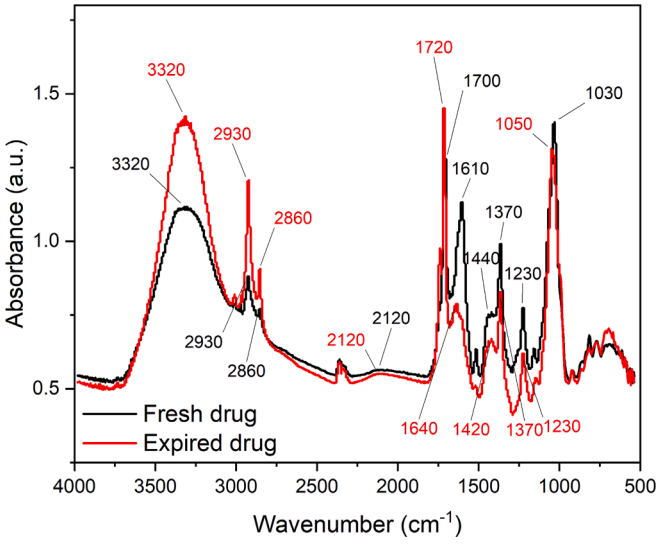

Fig. 1. FTIR spectra of the fresh and expired remdesivir drug.

Table 1
The chemical bonds related to each absorption peak for the fresh and expired drug.

Sample	Wavenumber (cm^{-1})	Chemical bond(s)	Ref.
Fresh drug	3320	ν(O–H)/ ν(N–H)	[39,40]
	2930	ν(C–H)	[40,41]
	2860	ν(C–H)	[40,41]
	2120	ν(C≡N)	[42]
	1700	ν(C=O)	[43]
	1610	ν(C=C)/δ(N–H)	[39,44]
	1440	δ(C–H)	[45,46]
	1370	δ(C–H)	[45]
	1230	ν(C-N)	[42]
	1030	ν(C-O)	[39,47]
Expired drug	3320	ν(O–H)/ ν(N–H)	[39,40]
	2930	ν(C–H)	[40]
	2860	ν(C–H)	[40,48]
	2120	ν(C≡N)	[42]
	1720	ν(C=O)	[43]
	1640	ν(C=C)/δ(N–H)	[39,44]
	1420	δ(C–H)	[49]
	1370	δ(C–H)	[49]
	1230	ν(C-N)	[42]
	1050	ν(C-O)	[39,50]

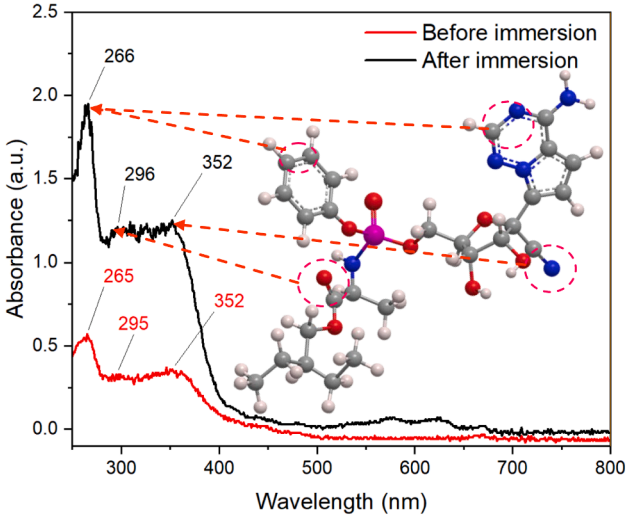

Fig. 2. UV–Vis plots of the corrosive solution with ERD before and after 48 h immersion of an St12 plate.

some of the drug molecules present in the solution have reacted with corrosion products of the steel, such as iron cations, forming insoluble organic–metallic complexes in the acidic electrolyte. These complexes deposit on the submerged electrode surface, forming a dense layer. The presence of this protective layer will be further characterized through electrochemical tests and additional analyses.

Electrochemical observations

OCP test

To evaluate the thermodynamic stability of the samples, OCP (open-circuit potential) values for St12 coupons in the acidic medium were measured in the presence of different dosages of the SAA, and the resulting curves are displayed in Fig. 3. The shift of OCP values toward more negative values over time for the immersed St12 coupon in the AA-free HCl solution can be explained by the fact that the pre-existing oxide film on the surface of the soaked steel plates can break down due to the aggressive nature of the acidic environment [59,60]. As a result, active sites (such as defects, grain boundaries, or imperfections) on the St12 surface become exposed to the solution. These active sites are more susceptible to metal dissolution (corrosion) compared to the pre-existing oxide film, and thus, the soaked electrode exhibited more active behavior with increasing immersion time. However, the decreasing trend in OCP values has been less pronounced in the SAA-containing samples compared to the blank sample, indicating the formation of a new organic film on the electrode surface [61]. The fluctuations in the OCP diagram of the St12 immersed in the SAA-containing HCl solutions arise from dynamic processes occurring at the St12-HCl interface. Specifically, the inhibitor film may break down due to localized aggressive species (e.g., Cl^-), and as the film weakens, the OCP fluctuates during the immersion period.

By comparing the obtained OCP values for the SAA-containing samples with the blank sample, it is clear that the values shifted to a less negative range with longer immersion times due to the dominance of anodic inhibition by the ERD. In addition, it can be observed that thermodynamic stability was achieved after approximately 1000 s of immersion.

EIS measurements

EIS tests were performed at different immersion time intervals (45, 90, 270, 580, and 1080 min) to investigate the anti-corrosion behavior of the immersed St12 sheets in the SSA-containing solutions. Fig. 4 and Fig. S1 (in the supplementary information file) show the Nyquist and Bode curves for different ERD dosages, respectively.

According to the semicircle shape in Nyquist diagrams (Fig. 4), it can be concluded that corrosion reactions are under the control of the charge transfer process [62]. Additionally, the increase in the diameter of the Nyquist semicircles at higher dosages of the SAA indicates that the adsorption of the ERD molecules on the St12/electrolyte interface and the formation of a barrier layer on the active areas of the metal surface are the main mechanisms of inhibition [63–65]. By modeling the experimental data with the equivalent circuit known as Randles cell ($R_s(Q_{dl}R_{ct})$), the values of the electrochemical parameters were obtained, and the inhibition percentage (η%) was calculated using Eq. (1) [66,67]:

$$\eta\% = [(R^i_{ct} - R^0_{ct}/R^i_{ct})] \times 100 \quad (1)$$

The obtained electrochemical parameters are reported in Table 2.

From Table 2, it can be observed that the values of *Rs* for the SAA-containing samples were lower than those obtained for the blank sample. This can be attributed to the fact that the release of $Fe2^+$ cations (corrosion products) into the solution in samples with lower dosages of SAA increases the solution conductivity. Therefore, the lower corrosion rate with increasing SAA concentration leads to a reduction in the number of cations and an increase in the electrolyte resistance. From the charge transfer variations for the blank sample, it can be seen that the parameter's value decreased from approximately 37 Ω·cm⁻1 at 45 min to around 19 Ω·cm⁻1 after 1080 min of immersion, indicating that the aggressive solution attacked the immersed St12 coupon. In addition, the increasing trend of R_{ct} values with higher SAA dosages in the corrosive solution demonstrates the successful adsorption of organic molecules on the St12 surface. Furthermore, at higher inhibitor dosages dissolved in the corrosive environment, the values of the "*n*" parameter showed an increasing trend, indicating that the surface roughness decreases in the presence of more SAA molecules. The values of C_{dl} can be calculated using Eq. (2) [68].

$$C_{dl} = (Y_{o,dl})^{(1/n)} x \left[\frac{R_{ct} \times R_s}{R_{ct} + R_s}\right]^{((1-n)/n)} \quad (2)$$

Based on Table 2, it can be observed that higher SAA dosages result in lower C_{dl} values, indicating the replacement of water molecules by organic molecules of the ERD [69]. In fact, the reduction in water-metal interactions in the presence of the adsorbed organic layer on the

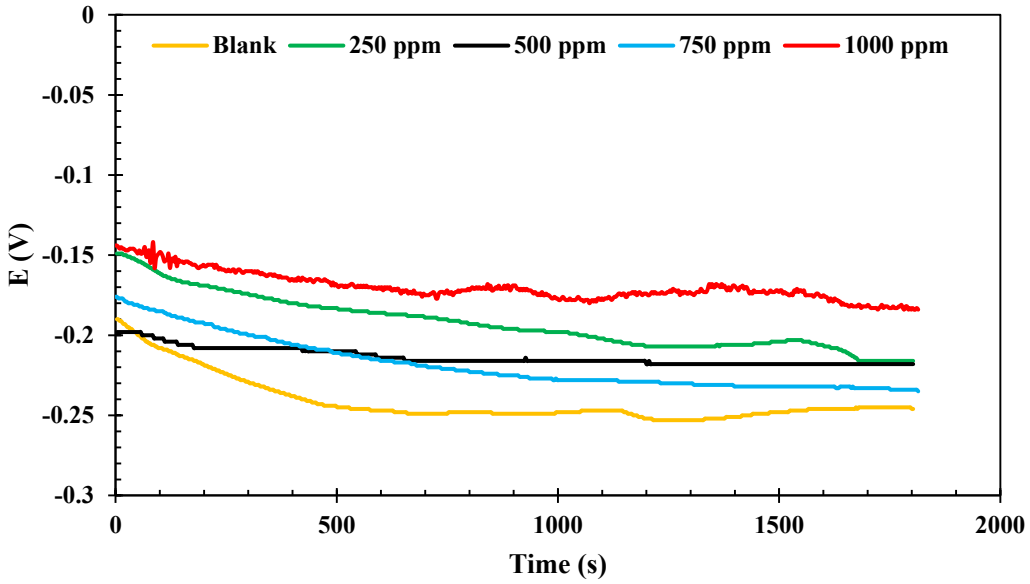

Fig. 3. OCP diagrams of the immersed St12 in the HCl solution with 0, 250, 500, 750, and 1000 ppm EDR.

submerged electrode decreases the electrical double-layer thickness, resulting in a lower capacitance value. On the other hand, it is well known that the dielectric constant of water is higher than that of the SAA structure. Therefore, the replacement of water molecules with SAA molecules leads to a decrease in the equivalent capacitance value of the double-layer (C_{dl}). Furthermore, the reported data show an improvement in the inhibition efficiency (η%) with increasing SAA concentration. Indeed, at higher concentrations, more inhibitor molecules are available for adsorption, and this increased adsorption enhances the coverage of the St12 surface, reducing its exposure to corrosive agents. Achieving an inhibition efficiency of more than 97 % in the presence of 1000 mg per liter of the expired Remdesivir drug indicates its excellent inhibition performance as an SAA for steel in an acidic environment. This value surpasses many previous studies on eco-friendly inhibitors.

PDP analysis

The PDP curves of St12 coupons immersed in 1 M HCl solution containing different concentrations of expired Remdesivir drug (ERD) for 1080 min are shown in Fig. 5. The electrochemical parameters extracted from Tafel extrapolation, including E_{corr}, i_{corr}, βa and βc, Rp, and CR, are summarized in Table 3.

In comparison with the blank sample, the addition of the SAA up to 1000 ppm caused a significant transfer of the anodic branch towards lower current density values, leading to the decrease in the i_{corr} value. It can also be seen that the values of E_{corr} shift toward more positive values (anodic shift). However, no significant changes are observed in the cathode branch, indicating the dominance of anodic inhibition, especially at lower concentrations. By comparing the PDP curves of the samples immersed in solutions with 250 to 750 ppm, it is observable that with the increase of the SAA dosage, the E_{corr} slightly moves towards more negative (cathodic) potentials, causing a decrease in the i_{corr} due to major changes in the cathodic branch. In other words, within this range of SAA concentration, the cathodic performance of the inhibitor is dominant. The comparison of PDP curves between the blank sample and ERD-containing solutions demonstrates a significant reduction in i_{corr} with increasing inhibitor concentration, confirming the adsorption of ERD molecules onto the metal surface. The decrease in icorr is most significant in the presence of 1000 ppm ERD, where a value of 0.0479 μA/cm^2 was recorded, corresponding to a corrosion rate reduction of over 96 % compared to the blank sample.

The polarization resistance (R_p) quantifies the ease with which electrons flow across the electrode–electrolyte interface and is inversely proportional to the corrosion rate (CR). According to Table 3, higher polarization resistance and lower corrosion rate values with higher dosages of the SAA indicate better protective performance of the inhibitor-formed film and lower kinetics of the electrochemical reactions responsible for corrosion. The highest polarization resistance (about 829 Ω.cm^2) and lowest corrosion rate (about 0.544 mpy) were observed in the sample containing 1000 ppm of ERD.

Regarding the corrosion potential, a shift toward more positive values is observed in the presence of ERD, indicating that the inhibitor primarily suppresses anodic reactions. However, at intermediate inhibitor concentrations (250–750 ppm), E_{corr} slightly shifts in the cathodic direction, suggesting a minor influence on the cathodic hydrogen evolution reaction. According to the NACE standard classification, if E_{corr} shifts by more than 85 mV, the inhibitor is categorized as a mixed-type inhibitor [70]. However, in this study, the observed shifts in E_{corr} are below this threshold, confirming that ERD predominantly acts as an mixed-type inhibitor by interfering with the dissolution of iron into Fe^{2+} ions.

The Tafel slopes (βa and βc) provide further insight into the inhibition mechanism. The βa values decrease with increasing inhibitor concentration up to 750 ppm, suggesting that ERD molecules hinder the oxidation of Fe to Fe^{2+} by forming a protective layer. The slight variation in βc values, particularly at higher concentrations, indicates that the inhibitor has a lesser impact on the cathodic reaction mechanism. At 1000 ppm, βa significantly increases, which may be attributed to the thickening of the inhibitor layer, causing diffusion-controlled mass transport effects.

Polarization resistance is inversely proportional to the corrosion rate and provides insight into the protective efficiency of the inhibitor film. As shown in Table 3, Rp increases significantly with increasing ERD concentration, reaching a maximum of 829.584 Ω.cm^2 at 1000 ppm, which is nearly 40 times higher than the blank sample (20.863 Ω.cm^2). This confirms the strong protective effect of ERD against corrosion by forming a stable and adherent layer on the metal surface.

The corrosion rate (CR) follows a decreasing trend with increasing ERD concentration. In the absence of ERD, the corrosion rate is 14.714 mpy, which drastically reduces to 0.544 mpy at 1000 ppm, demonstrating the exceptional inhibition performance of ERD in acidic environments. This significant reduction suggests that ERD efficiently blocks the active corrosion sites on the St12 surface, preventing direct interaction between aggressive Cl^- ions and the metal substrate.

The efficiency of ERD as a corrosion inhibitor is closely related to its

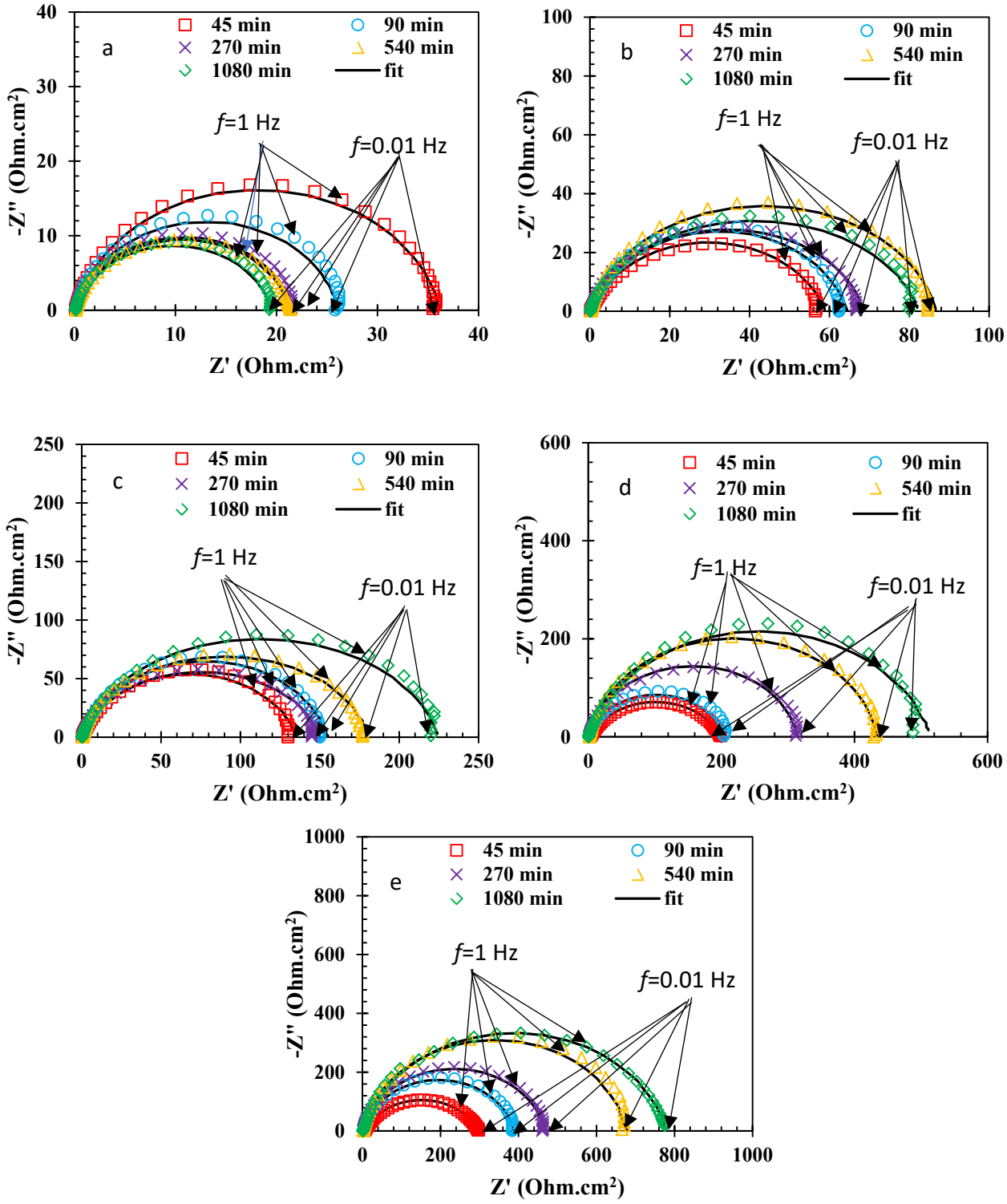

Fig. 4. Nyquist plots of (a) blank and ERD-containing samples with concentrations of (b) 250, (c) 500, (d) 750, and (e) 1000 ppm immersed for various durations.

adsorption onto the metal surface. The adsorption process is governed by the nature of the inhibitor molecules and their interaction with metal atoms. The presence of functional groups such as C=O, C-N, N–H, and P=O in ERD facilitates the formation of coordinate bonds with Fe atoms, leading to the formation of a protective layer. Additionally, the presence of π-electrons in the aromatic rings enhances physisorption interactions, further improving inhibition efficiency.

The inhibition efficiency of ERD (97.3 % at 1000 ppm) surpasses that of other expired drug-based inhibitors reported in the literature. For example, expired Ranitidine exhibited an inhibition efficiency of 89 % for aluminum in HCl [27], while expired Amoxicillin achieved an efficiency of 94.5 % for mild steel [30]. This superior performance may be attributed to the multiple active sites in the remdesivir structure, enabling strong adsorption and enhanced protective layer formation.

Adsorption isotherms

The stronger corrosive effect on the CR of the St12 coupons in the

Table 2
The obtained electrochemical parameters from data modeling of the EIS results.

Dos. (ppm)	Duration (min)	R_s (Ohm.cm^2)	$CPE_{db}Y_0$ (mS.sec^n/cm^2)	n	R_{ct} (Ohm.cm^2)	C_{dl} (F/cm^2)	η%	X^2
	45	0.276 ± 0.010	3.65 ± 0.12	0.85 ± 0.02	36.65 ± 2.34	12.35 ± 0.10	–	3.21×10^{-3}
	90	0.251 ± 0.009	4.99 ± 0.21	0.84 ± 0.01	26.87 ± 3.76	19.38 ± 0.15	–	2.41×10^{-3}
0	270	0.250 ± 0.008	5.19 ± 0.22	0.82 ± 0.02	23.50 ± 1.49	24.98 ± 0.13	–	1.98×10^{-3}
	540	0.346 ± 0.018	5.99 ± 0.17	0.82 ± 0.02	22.32 ± 2.21	31.91 ± 0.22	–	9.39×10^{-4}
	1080	0.245 ± 0.025	6.02 ± 0.16	0.79 ± 0.01	19.05 ± 3.00	41.73 ± 0.21	–	3.09×10^{-3}
	45	0.376 ± 0.019	3.02 ± 0.09	0.86 ± 0.02	59.17 ± 3.17	9.48 ± 0.29	38.06 ± 2.32	3.88×10^{-3}
	90	0.402 ± 0.019	2.99 ± 0.10	0.85 ± 0.01	61.69 ± 3.49	10.44 ± 0.18	56.44 ± 1.29	5.23×10^{-3}
	270	0.309 ± 0.033	2.76 ± 0.09	0.85 ± 0.01	63.64 ± 4.09	9.07 ± 0.17	63.07 ± 3.33	8.83×10^{-4}
250	540	0.287 ± 0.022	2.09 ± 0.11	0.84 ± 0.02	80.02 ± 3.98	7.06 ± 0.09	72.11 ± 3.12	1.36×10^{-3}
	1080	0.142 ± 0.012	1.87 ± 0.08	0.84 ± 0.02	82.71 ± 3.12	5.41 ± 0.08	76.97 ± 1.23	6.43×10^{-3}
	45	0.765 ± 0.010	2.98 ± 0.31	0.85 ± 0.01	135.34 ± 13.09	11.65 ± 0.87	72.92 ± 0.99	3.88×10^{-3}
	90	0.325 ± 0.011	2.34 ± 0.14	0.85 ± 0.02	144.65 ± 15.34	7.54 ± 0.12	81.42 ± 1.23	7.21×10^{-4}
500	270	0.444 ± 0.013	1.88 ± 0.04	0.87 ± 0.02	151.77 ± 16.05	5.13 ± 0.55	84.52 ± 1.99	4.38×10^{-3}
	540	0.523 ± 0.012	1.76 ± 0.25	0.89 ± 0.01	174.12 ± 21.21	4.09 ± 0.78	87.18 ± 0.89	6.10×10^{-3}
	1080	0.504 ± 0.010	1.55 ± 0.10	0.9 ± 0.03	226.88 ± 10.98	3.25 ± 0.98	91.60 ± 1.28	5.41×10^{-4}
	45	0.623 ± 0.014	2.60 ± 0.18	0.86 ± 0.03	195.11 ± 23.76	8.65 ± 0.32	81.22 ± 1.20	1.45×10^{-3}
	90	0.633 ± 0.021	2.17 ± 0.12	0.87 ± 0.01	209.76 ± 18.76	6.38 ± 0.65	87.19 ± 0.76	1.21×10^{-3}
750	270	0.602 ± 0.029	1.46 ± 0.21	0.89 ± 0.02	336.29 ± 10.87	3.37 ± 0.45	93.01 ± 0.87	2.87×10^{-3}
	540	0.651 ± 0.022	1.11 ± 0.12	0.91 ± 0.01	453.87 ± 23.80	2.13 ± 0.47	95.08 ± 0.67	8.99×10^{-4}
	1080	0.453 ± 0.019	0.99 ± 0.09	0.92 ± 0.03	546.06 ± 20.09	1.68 ± 0.19	96.51 ± 1.12	3.70×10^{-3}
1000	45	0.424 ± 0.029	1.82 ± 0.22	0.87 ± 0.03	389.79 ± 13.05	4.91 ± 0.17	90.60 ± 1.11	1.64×10^{-3}
	90	0.398 ± 0.032	1.12 ± 0.11	0.88 ± 0.03	399.89 ± 17.54	2.57 ± 0.21	93.28 ± 1.98	3.85×10^{-3}
	270	0.432 ± 0.039	1.03 ± 0.15	0.89 ± 0.02	456.89 ± 17.45	2.19 ± 0.17	94.86 ± 0.98	4.93×10^{-3}
	540	0.421 ± 0.082	0.76 ± 0.07	0.91 ± 0.02	683.76 ± 21.21	1.34 ± 0.12	96.74 ± 1.34	9.71×10^{-4}
	1080	0.523 ± 0.021	0.69 ± 0.11	0.92 ± 0.03	786.03 ± 23.00	1.15 ± 0.15	97.58 ± 1.39	8.65×10^{-4}

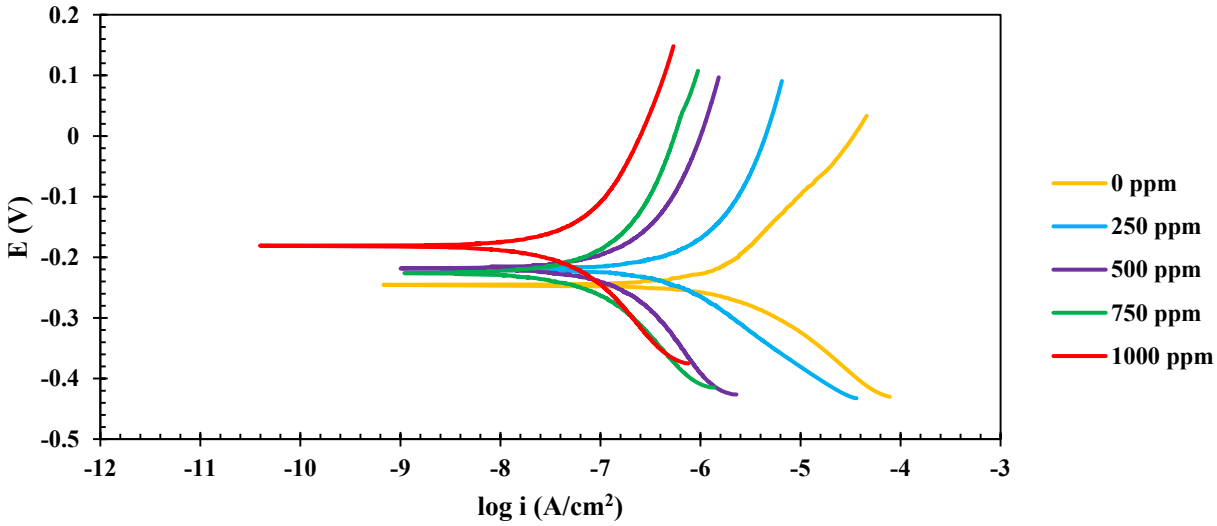

Fig. 5. The PDP curves of St12 coupons soaked in the corrosive electrolyte containing different dosages of the SAA for 1080 min.

Table 3
Tafel extrapolated parameters from PDP curves.

AA dosage (ppm)	β_a (V/dec)	$-\beta_c$ (V/dec)	E_{corr} vs SCE (V(	i_{corr} (μA/cm^2)	Rp(Ohm.cm^2)	CR (mmy)
0	0.1729 ± 0.004	0.1172 ± 0.004	−0.245 ± 0.01	1.2949 ± 0.05	20.863 ± 4.49	14.714 ± 0.04
250	0.1356 ± 0.004	0.1175 ± 0.004	−0.219 ± 0.01	0.3289 ± 0.05	83.105 ± 4.49	3.737 ± 0.04
500	0.1388 ± 0.004	0.1088 ± 0.004	−0.220 ± 0.01	0.1147 ± 0.05	261.289 ± 4.49	1.303 ± 0.04
750	0.1391 ± 0.004	0.1202 ± 0.004	−0.226 ± 0.01	0.0626 ± 0.05	529.394 ± 4.49	0.711 ± 0.04
1000	0.2721 ± 0.004	0.1379 ± 0.004	−0.181 ± 0.01	0.0479 ± 0.05	829.584 ± 4.49	0.544 ± 0.04

presence of lower SAA dosages confirms the adsorption of ERD molecules on the electrode. In this context, adsorption isotherms provide valuable insights into the adsorption mechanism. The relationships between C/θ versus C and lnθ versus ln$C$ were utilized to calculate the Langmuir and Freundlich adsorption isotherms, respectively [53,71]. As shown in Fig. 6, the regression coefficient values for the Langmuir and Freundlich adsorption models were 0.99 and 0.95, respectively, indicating that the adsorbed SAA occupies only one active site on the St12/electrolyte interface [72,73].

FE-SEM/EDS/Map, AFM and CA results

Fig. 7 displays FE-SEM/AFM micrographs and CA images of the immersed electrode surface morphology in 1 M HCl electrolyte without and with 1000 ppm ERD.

The FE-SEM micrograph of the blank sample after immersion in the HCl medium reveals both general corrosion (uniform attack) and pitting corrosion, which increased the overall roughness of the electrode

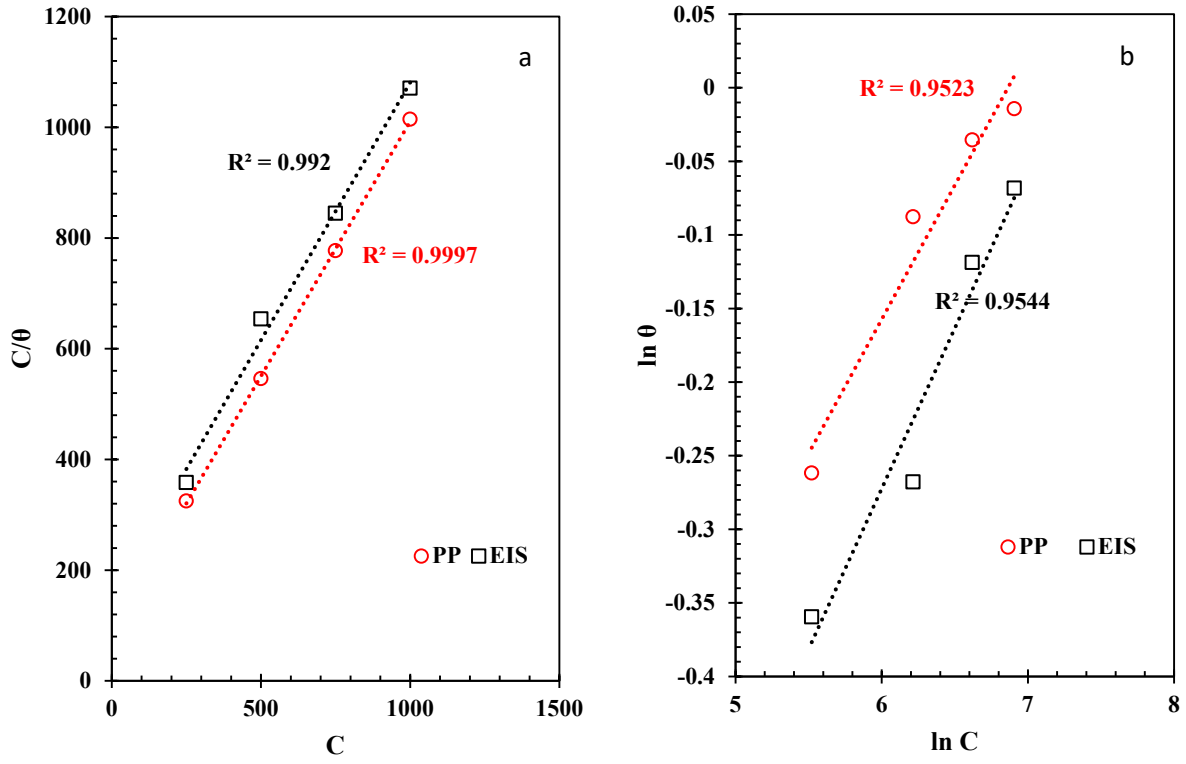

Fig. 6. .

surface. In contrast, the insoluble dense layer formed on the St12 surface in the presence of ERD reduced the surface roughness of the electrode. Using EDS and elemental mapping analyses, the formation of this layer on the St12 surface was verified (Fig. S2), where carbon, oxygen, nitrogen, and phosphorus elements, in addition to iron and chlorine, were detected on the St12 surface of the immersed coupon in the SAA-containing medium. AFM analysis provided valuable quantitative information about the topology of the immersed working electrode surface (Fig. 7 (c and f)). When the quantitative data for the sample containing 1000 ppm ERD were compared to those of the blank sample, it was found that the average roughness (R_a) of the SAA-containing sample was 35.5 nm, whereas the value for the blank sample was 128.9 nm. Therefore, the presence of a dense film on the St12 surface and the reduction in surface corrosion attack were confirmed by the lower values of the average roughness parameter in the presence of the SAA.

The contact angle of water droplets on a surface provides valuable insights into the surface chemistry of an immersed steel electrode in HCl solution, especially when considering the presence or absence of an anti-corrosion agent. According to Fig. 7 (b and e), the untreated steel surface (without the SAA) exhibits hydrophobic behavior (with an average contact angle of 65.5°) due to the presence of oxide layers and surface roughness. When the SAA forms a protective layer on the steel surface, the adsorbed organic molecules enhance the surface's hydrophilicity, thereby improving its wettability (with an average contact angle of 77.0°). A less hydrophilic steel surface promotes better corrosion inhibition because it limits the access of aggressive ions while allowing efficient ERD adsorption.

XPS analysis

XPS analysis was used to investigate the steel surface immersed in an HCl medium containing the expired Remdesivir, which contains carbon, nitrogen, oxygen, and phosphorus elements in its chemical structure. Fig. 8 represents the obtained XPS spectra for the St12 in the SAA-containing HCl medium.

The survey XPS spectrum (Fig. 8 (a)) revealed the presence of SAA-related elements on the surface of the submerged St12 in the SAA-containing medium. Accordingly, the atomic percentage values for C, O, N, Fe, P, and Cl elements were 60.31 %, 23.87 %, 8.34 %, 3.32 %, 2.82 %, and 1.34 %, respectively. The successful adsorption of expired Remdesivir drug molecules on the St12 surface is evident from the presence of these elements, which is consistent with previous experimental results. The low atomic percentage of Fe can be attributed to the fact that XPS is a surface-sensitive technique, probing only the top few nanometers of the material. In the presence of a relatively thick protective film, the Fe element may not contribute significantly to the detected signal. Additionally, the detection of chlorine can be attributed to the adsorption of Cl^- from the HCl solution on the electrode surface.

In the high-resolution O 1 s spectrum (Fig. 8 (b)), the deconvoluted peaks at 527.72, 528.38, 529.32, and 533.03 eV can be assigned to Fe-O (10.97 %At.), P=O/C-O (50.38 %At.), P-O (37.05 %At.), and C=O (1.60 %At.), respectively. From Fig. 8 (c), the peaks at 712.63, 715.11, 726.29, and 730.73 eV can be assigned to Fe^{2+} $2p_{1/2}$ (43.58 %At.), Fe^{3+} $2p_{1/2}$ (21.31 %At.), Fe^{2+} $2p_{3/2}$ (19.75 %At.), and Fe^{3+} $2p_{3/2}$ (15.35 %At.), respectively. In the initial stages of corrosion, iron (Fe) reacts with oxygen (O_2) to form Fe^{2+} ions, while Fe^{3+} ions are formed by the oxidation of Fe^{2+} ions or directly from the metal surface.

The C 1 s high-resolution peak (Fig. 8 (d)) was deconvoluted into five peaks at 281.86, 282.38, 283.59, 285.08, and 285.39 eV, corresponding to C–H/C=C (53.73 %At.), C=N (21.22 %At.), C-N/C-O (6.24 %At.), C≡N (2.47 %At.), and O-C=O (16.34 %At.), respectively. The detection of the C≡N bond, a characteristic bond of Remdesivir molecules, along with other bonds in the chemical structure of the expired drug on the steel surface, is consistent with FTIR and UV–Vis results, confirming the formation of a layer of these molecules on the soaked St12 electrode.

As can be seen in Fig. 7 (e), N 1 s high-resolution peak was deconvoluted into 3 peaks at 395.77, 396.76, and 397.08 eV, attributing to C-N/C≡N (36.64 % At.), C=N (57.05 % At.), N-Fe (6.31 %At.), respectively [74]. The formation of the N-Fe bond indicates the formation of a coordinate bond between nitrogen (a heteroatom in the chemical

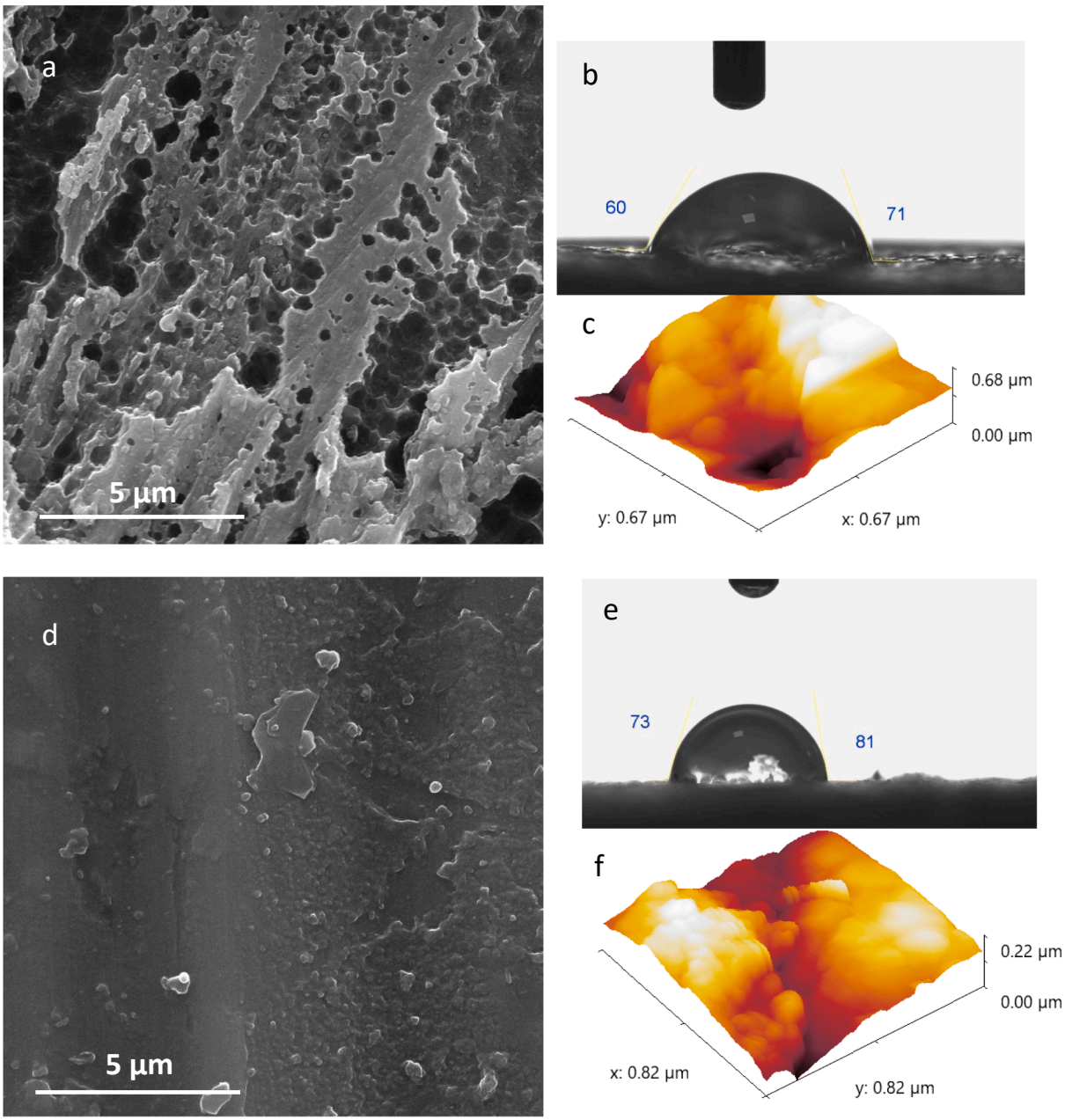

Fig. 7. FE-SEM, CA, and AFM images of the (a, b, and c) blank sample and (d, e, and f) SAA-containing sample.

structure of the expired drug) and Fe on the surface of the immersed coupon. Therefore, the XPS results clearly demonstrate the successful formation of a protective layer of expired Remdesivir drug molecules on the steel surface.

Results of QCCs

The chemical reactivities possessed Remdesivir molecule is calculated with QCCs based on DFT for useful elucidation of anti-corrosion potentials of the molecule. The results of electronic structure of Remdesivir molecule optimization are presented in Fig. 9 below. Molecular orbital structures generated from geometrical optimization provide information on the specific roles in evaluating the molecule reactivities and adsorption potentials of the molecule on St12 surface. The results of total electron density revealed that Remdesivir molecule that electron was evenly distributed round the molecule, thus indicating either flat-lying position or total saturation. The structure of HOMO reflects the regions within the molecule that has potentials to bequeath electrons to sites of electrophilicity, thus it represents the locations of nucleophilic reaction where metal-inhibitor adsorption interaction manifests [53,75]. It is clearly seen that electrons are distributed heavily around the region with more of presence nitrogen atoms and carbon–oxygen bonds. The structure LUMO of Remdesivir molecule reflects the region within the molecule where it is at ease to receive electron from the metal surface [53]. Also, it is seen that electrons were much concentrated at region containing benzene group, phosphorus atom, carbon–nitrogen bonds. Furthermore, careful examination on the position of HOMO and LUMO structure of Remdesivir molecule revealed that there was no overlap rather each orbital maintained its specific and stronger interaction within its region to ensure effective inhibition performance of the molecule. Furthermore, remdesivir is a nucleoside analog, and its molecule structure consists of a nucleoside base linked to a sugar moiety and a phosphate group. The protonated structure of remdesivir contains several functional groups, including: (i) amino

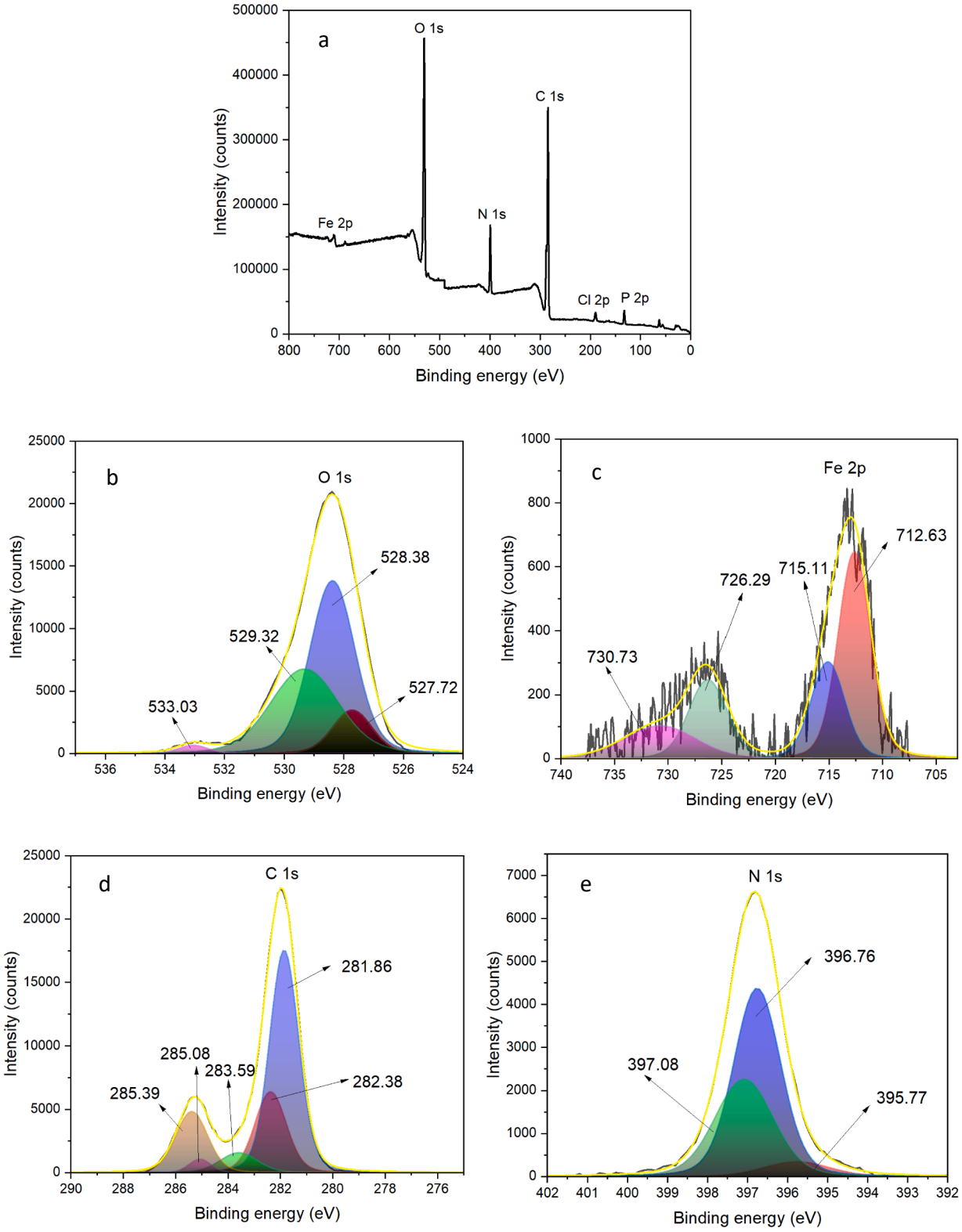

Fig. 8. (a) Overall spectrum and high-resolution spectra of (b) O 1 s, (c) Fe 2p, (d) C 1 s, and (e) N 1 s.

group (–NH2), (ii) hydroxyl group (–OH), (iii) phosphate group (−PO4), (iv) carbonyl group (−C=O) and (v) amide group (–CONH-). The chemical structure of remdesivir is $C_{27}H_{35}N_6O_8P$ when protonated the formula becomes $C_{27}H_{36}N_6O_8P^+$, thus, indicating that the nitrogen atoms in the nucleoside base and the phosphate group are protonated, resulting in a positively charged ammonium ion. More interestingly, the exact site of protonation can vary depending on the pH and charge environment. But the nitrogen atoms in the amide groups or the phosphoramidate group are the most likely sites because it has lone pairs and can be a ligand in a complex or complex ion. The protonation introduce

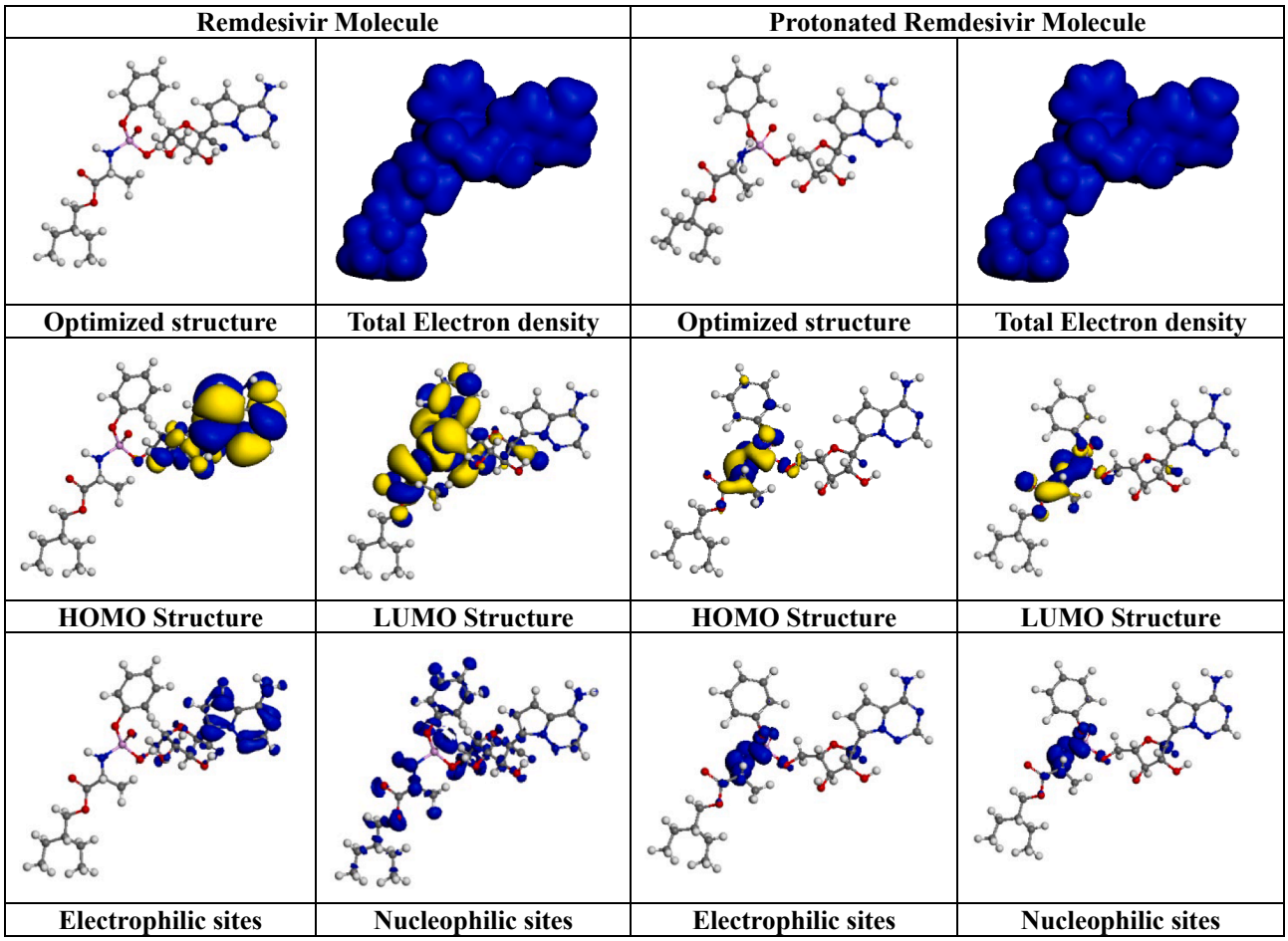

Fig. 9. Geometrical optimized electronic structure of Remdesivir molecule and Protonated molecule: Yellow isosurface stands for electron loss. Blue isosurface stands for electron buildup and atoms legend: C- Gray, O – Red, H – White, P – Purple. (For interpretation of the references to colour in this figure legend, the reader is referred to the web version of this article.)

a positive charge which affect the molecule's interaction with other species including metal surface, etc. Evidently, it is seen that phosphoramidate group within the remdesivir molecule is situated around the HOMO and LUMO regions of the optimized molecule. Thus, indicating the positions where the protonated molecule is at ease to donate and welcome electron from the metal surface (Fig. 10).

Quantum reactivity parameters

Quantum chemical parameters are essential for evaluating the stable performance and reliability response of molecule regarding of its ability in inhibiting the metal corrosion process via adsorption technique. Results of some chemical parameters obtained are illustrated in Table 4 below.

Information concerning the chemical reactivities possessed by Remdesivir molecule is presented in Table 4 It is acknowledged that calculated values of other QCC parameters possessed by the molecule were determined from the values of E_{HOMO} and E_{LUMO}. Equally, it is observed that E_{HOMO} and E_{LUMO} of Remdesivir molecule possess high (−5.3974 eV) low (−3.2932 eV) values respectively, thus showing balanced ability of the molecule in donating and accepting electrons for metal surface-inhibitor adsorption. High E_{HOMO} value of the molecule obtained indicates its good potentials to offer or donate electron to empty molecular orbital and lower value E_{LUMO} confirms the evidence of the molecule to accept electron. The energy gap value of 2.1042 eV was obtained and this predicts the effective anti-corrosion potential of the molecule as observed in the results of the experimental data. The index of electronegativity is used to assess the electron receiving ability of a molecule and 4.3453 eV electronegativity value obtained confirms the good electron accepting characteristics possessed by the molecule for efficient metal surface-inhibitor adsorption. The hardness or softness nature of molecule plays significant role during chemical reaction of the molecule with other substance or electrolytes as the stability and resistance to polarization of the molecule is dependent on the nature of molecule. Data in Table 4 presents that Remdesivir molecule has soft nature showing good potential for corrosion inhibitor during metal surface-inhibitor adsorption. Electrophilicity and nucleophilicity value respectively present the extent of attack on a molecule during chemical reaction and they are related directly to electron transfer (donating and accepting) capability of inhibiting molecule. In addition, higher ω^+ value associates with enhanced electron accepting control and lower ω^- value associate with good electron donating control of inhibiting molecule. The result in Table 4 showed that Remdesivir molecule is more of electron donating than electron accepting molecule. The ΔN value measures the stable response of a molecule during chemical reaction as a result of electron transfer between the molecule and St12 surface. Remdesivir molecule showed a positive ΔN value which is less than 1.6 eV, indicating stable response of electron transfer between the Remdesivir molecule and empty orbitals of metal surface. Conclusively, $\Delta E_{b\text{-}d}$ value obtained is lower than zero, suggesting favorable energetic electron transfer between the Remdesivir molecule and St12 surface. In addition, the information concerning the chemical reactivities possessed by protonated Remdesivir molecule as presented in Table 4 revealed that protonated form of the molecule possessed better characteristic features responsible for the corrosion inhibition compared to

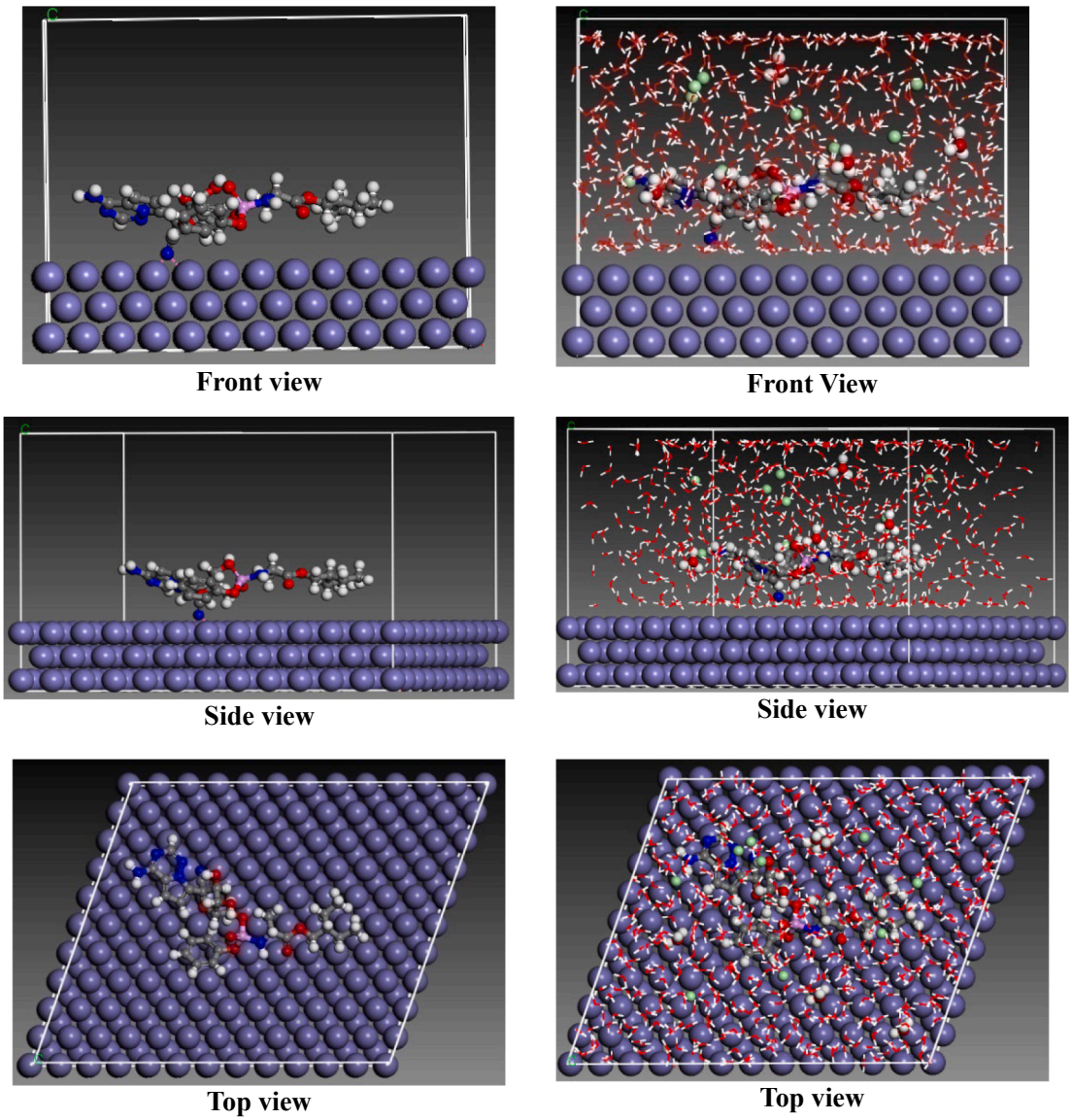

Fig. 10. Configurations of stable adsorption of mild steel crystal surface [110] and Remdesivir molecule with and electrolytic constituents in different views.

Table 4
Computed QCC reactivities of Remdesivir molecule and Protonated molecule.

S/N	Mathematical representation [2–4]	Calculated values (eV)	Calculated values (eV) for Protonated molecule
1	E_{LUMO}	−3.2932	−4.4370
2	E_{HOMO}	−5.3974	−4.6983
3	$\Delta E_{gap} = E_{LUMO} - E_{HOMO}$	2.1042	0.2613
4	$A = -E_{LUMO}$	3.2932	4.4370
5	$I = -E_{HOMO}$	5.3974	4.6983
6	$\chi = -(E_{LUMO} + E_{HOMO})/2$	4.3453	4.5677
7	$\eta = (E_{LUMO} - E_{HOMO})/2$	1.0521	0.1307
8	$\sigma = 1/\eta$	0.9505	7.6511
9	$\omega = \chi^2/2\eta$	8.9733	79.8159
10	$\in = 1/\omega$	0.1114	0.0125
11	$\omega^+ = (I + 3A)^2/16(I - A)$	6.9322	78.9505
12	$\omega^- = (3I + A)^2/16(I - A)$	11.2775	82.1449
13	$\Delta N = \phi - \chi/2\eta$	0.2208	0.9269
14	$\Delta E_{back-donation} = -(\eta/4)$	−0.2630	−0.0327

*Note: Mild steel surface work function, ϕ_{Fe} considered = 4.81 eV [4].

Remdesivir in ordinary state. Finally, the essence of employing the theoretical computations in this work is to explore the co-relation between the inhibitive performance of the molecule and its molecular structure. Also, the significance of the theoretical data obtained in this work is to revalidate the experimental results and to explain the experiment results from the molecular point of view.

Molecular dynamic simulation (MDS)

The MDS techniques was utilized for investigation Remdesivir molecule and metal crystal surface Fe (110) adsorption strength at molecular level in order to provide proper and better stable interaction understanding between them. The investigation was carried out in both gaseous phase and solvated (approximated experimental environment) to predict the effect of electrolytic constituents on the adsorption inhibition characteristics. The existing interactive strength or the adsorption strength on metal surface-inhibitor at the interfacial medium is determined by the binding energy parameter, and the negative value of the parameter suggests more spontaneous process with probable strong and durable metal surface-inhibitor interaction. The binding energy results obtained for Remdesivir molecule in gaseous and solvated phase are −205.69 and −144.314 kcal/mol respectively. Fig. 9 presents the

different views of the most stable configuration obtained from the adsorption between metal surface and inhibitor molecule with observed flat-lying position of Remdesivir molecule on the metal surface. This suggests evidence of favorable interaction of metal surface-inhibitor adsorption. Equally, the region within the Remdesivir molecule dominated by nitrogen atom is believed to be responsible for donation of lone pair electron which formed coordinated bond with partial filled 3-d orbital on the St12 surface resulting to stable protective film layer. Hence, the film layer modifies the surface chemical on the St12 surface by blanketing some of the corrosion active sites on the surface. Furthermore, the presence of benzene structure is also believed to be π-electron cloud which contributed in forming physical film for surface metal protection. Non-polar regions in the inhibitor molecule together with protonated inhibitor species caused by the constituents of electrolytic system offered some hydrophobic characteristics which assisted in displacement of molecules on the St12 surface and proffer efficient metal protection in return [76]. Conclusively, we believed these outlined factors contributed immensely and effectively in the values of binding energy determined.

The strong correlation between theoretical quantum data and experimental results underscores the reliability and accuracy of the computational methods used in this study. This alignment validates the theoretical models employed, confirming their capability to accurately predict the structural and electronic properties of the investigated system. Furthermore, such consistency enhances the predictive power of quantum calculations, enabling the optimization of experimental procedures and reducing the need for extensive trial-and-error approaches. Additionally, the agreement between theory and experiment supports a deeper understanding of the underlying mechanisms, ensuring that the employed methodologies effectively capture the essential physicochemical interactions within the system.

Mechanism of corrosion inhibition of expired remdesivir

The corrosion inhibition mechanism of ERD on St12 steel in a 1 M HCl environment can be elucidated through a combination of experimental observations, electrochemical analyses, and theoretical computations. The following discussion integrates the findings from FTIR, UV–Vis, electrochemical tests, adsorption isotherms, DFT, and MDS to provide a comprehensive understanding of the inhibition mechanism.

The FTIR and UV–Vis spectra of both fresh and expired Remdesivir confirm that the chemical structure of the drug remains largely intact even after expiration. The presence of functional groups such as C≡N, C-N, C=O, N–H, and C-O in both samples indicates that the key reactive sites responsible for adsorption on the metal surface are preserved. However, the slight decrease in peak intensity of methyl and methylene groups, along with the increased intensity of the hydroxyl bond in the expired sample, suggests partial hydrolysis due to environmental factors like moisture and sunlight. Despite these minor changes, the expired drug retains its ability to act as an effective corrosion inhibitor. The adsorption of ERD molecules on the St12 steel surface is primarily driven by the presence of heteroatoms (N, O, P) and multiple bonds (C=O, C≡N, C-N) in its structure. These functional groups facilitate the formation of coordinate bonds with the iron atoms on the steel surface, leading to the creation of a protective organic film. The adsorption process is further supported by the Langmuir and Freundlich isotherms, which indicate that the inhibitor molecules occupy active sites on the steel surface, forming a monolayer that blocks the corrosive agents from reaching the metal.

The DFT calculations reveal the electronic structure and reactivity of the Remdesivir molecule, providing a molecular-level understanding of its inhibition mechanism. The high HOMO (highest occupied molecular orbital) energy (−5.3974 eV) indicates the molecule's ability to donate electrons to the metal surface, while the low LUMO (lowest unoccupied molecular orbital) energy (−3.2932 eV) suggests its capacity to accept electrons from the metal. The narrow energy gap (2.1042 eV) further confirms the molecule's high reactivity and strong adsorption potential. The protonated form of Remdesivir, which is likely to exist in the acidic environment, enhances its interaction with the steel surface. The positively charged ammonium ions (from protonated nitrogen atoms) and the phosphate group facilitate the formation of stable complexes with iron cations, leading to the deposition of insoluble organic–metallic compounds on the steel surface. This process is supported by the MDS results, which show a strong binding energy (−205.69 kcal/mol in the gaseous phase and −144.314 kcal/mol in the solvated phase) between the inhibitor and the Fe (110) surface. The flat-lying orientation of the Remdesivir molecule on the metal surface maximizes the coverage of active sites, further enhancing the protective effect.

The nucleoside analog structure of Remdesivir, with its multiple functional groups (amino, hydroxyl, phosphate, carbonyl, and amide), plays a critical role in its inhibition performance. The nitrogen and oxygen atoms in these groups act as electron donors, forming coordinate bonds with the iron atoms on the steel surface. Additionally, the benzene ring and phosphorus atom contribute to the molecule's ability to form π-electron interactions and hydrophobic layers, respectively, which further enhance the protective film's stability.

The protonation of the molecule in the acidic environment introduces positive charges that improve its adsorption on the negatively charged steel surface. The phosphoramidate group, located near the HOMO and LUMO regions, is particularly effective in facilitating electron transfer between the inhibitor and the metal, leading to the formation of a robust protective layer.

The combination of chemical adsorption, physical barrier formation, and electron transfer mechanisms contributes to the high η% of ERD, which exceeds 97 % at a concentration of 1000 ppm. The adsorbed inhibitor molecules not only block the active sites on the steel surface but also modify the electrochemical reactions responsible for corrosion. The reduction in CR and the increase in Rp with higher inhibitor concentrations further validate the effectiveness of the protective film.

Conclusion

In the wake of the COVID-19 pandemic, repurposing expired pharmaceuticals such as Remdesivir has emerged as a SAA for steel in an acidic environment. Our experimental results showed that at an optimum dosage of 1000 ppm, Remdesivir achieved a remarkable corrosion inhibition efficiency of over 97 %. This remarkable efficiency is attributed to the presence of nitrogen and oxygen heteroatoms and multiple benzene rings in Remdesivir's molecular structure, which facilitate strong chemisorption onto the St12 surface, forming a dense layer against corrosion. The modeling techniques further supported these findings by investigating the adsorption strength of the Remdesivir molecule on the Fe (110) metal crystal surface at a molecular level. The MDSs were conducted in both gaseous and solvated phases to approximate experimental conditions and predict the effect of electrolytic constituents on the adsorption inhibition characteristics. The binding energy results, −205.69 kcal/mol in the gaseous phase and −144.314 kcal/mol in the solvated phase, indicated a spontaneous and strong interaction between Remdesivir and the St12 surface, suggesting durable protection. The MDS results revealed a stable, flat-lying configuration of Remdesivir on the St12 surface, with nitrogen atoms in the molecule responsible for donating lone pair electrons to form coordinated bonds with the partially filled 3-d orbitals on the metal surface. This interaction results in the formation of a stable dense film, modifying the surface chemistry and blanketing active corrosion sites. Additionally, the benzene rings in Remdesivir contribute to the formation of a physical film through π-electron cloud interactions, enhancing surface protection. The presence of non-polar regions and protonated inhibitor species, influenced by the electrolytic system constituents, imparted hydrophobic characteristics to the film, displacing water molecules and providing efficient metal protection. These factors collectively contributed to the significant binding energy values observed and the high

corrosion inhibition efficiency achieved. In conclusion, this study not only highlights the innovative repurposing of expired Remdesivir as a highly effective SAA but also underscores the potential environmental and economic benefits of such an approach. The molecular insights provided by the MDS further validate the practical applicability of this method in enhancing the longevity and durability of metallic structures in acidic environments.

CRediT authorship contribution statement

Ismat H. Ali: Writing – original draft, Methodology, Investigation, Formal analysis, Conceptualization. **Ruhollah Sharifi:** Writing – review & editing, Visualization, Validation, Software, Data curation. **Ali Asghar Javidparvar:** Writing – review & editing, Writing – original draft, Supervision, Methodology, Data curation, Conceptualization. **Simeon C. Nwanonenyi:** Visualization, Validation, Resources, Investigation. **Emeka E. Oguzie:** Validation, Software, Resources, Investigation, Data curation. **Theodore A. Manfo:** Writing – review & editing, Writing – original draft, Validation, Supervision, Project administration, Methodology, Investigation, Conceptualization.

Declaration of competing interest

The authors declare that they have no known competing financial interests or personal relationships that could have appeared to influence the work reported in this paper.

Acknowledgement

The authors extend their appreciation to the Deanship of Research and Graduate Studies at King Khalid University for funding this work through Large Group Project under grant number (341/1445).

Appendix A. Supplementary data

Supplementary data to this article can be found online at https://doi.org/10.1016/j.jiec.2025.03.036.

References

[1] Y. Kim, S.J. Hwang, D. Kim, J. Park, Y. Kim, J. Kim, M. Bae, H. Hong, S. Park, J. Park, J.Y. Maeng, J. Lee, H.S. Park, J. Lee, Y. Piao, Adv Mater Interfaces 11 (2) (2024) 2300628, https://doi.org/10.1002/admi.202300628.
[2] K.E. Schneider, E.M. Martin, S.T. Allen, M. Morris, K. Haney, B. Saloner, S. G. Sherman, Int. J. Drug Policy 126 (2024) 104371, https://doi.org/10.1016/j.drugpo.2024.104371.
[3] G.-Q. Zhang, W. Liu, Y.-H. Shi, Y.-X. Zou, L.-Y. Xu, H.-L. Cheng, T. Wang, W.-B. Li, Y. Zhao, Z.-H. Xu, Microchem. J. 197 (2024) 109720, https://doi.org/10.1016/j.microc.2023.109720.
[4] S. Nhean, M.E. Varela, Y.-N. Nguyen, A. Juarez, T. Huynh, D. Udeh, A.L. Tseng, J Pharm Pract 36 (2) (2023) 407–417, https://doi.org/10.1177/08971900211048139.
[5] H.A. Blair, Drugs 83 (13) (2023) 1215–1237, https://doi.org/10.1007/s40265-023-01926-0.
[6] C. Chen, J. Fang, S. Chen, M.J.N. Rajaofera, X. Li, B. Wang, Q. Xia, BMC Infect Dis 23 (1) (2023) 672, https://doi.org/10.1186/s12879-023-08525-0.
[7] C. Sellitto, G. Corbi, N. Bertini, T. Ascione, M. Costantino, G. Scarpati, O. Piazza, A. Filippelli, V. Conti, P. Pagliano, J. Chemother. 35 (5) (2023) 383–396, https://doi.org/10.1080/1120009X.2022.2121091.
[8] D. Yan, B. Yan, Fundam Clin Pharmacol 37 (4) (2023) 726–738, https://doi.org/10.1111/fcp.12889.
[9] A. Rezapour, Z. Behroozi, M. Nasirzadeh, M. Rezaeian, M. Barzegar, M. Tashakori-Miyanroudi, A. Sayyad, A. Souresrafil, Infect Dis Poverty 12 (1) (2023) 39, https://doi.org/10.1186/s40249-023-01092-1.
[10] P.O. Godwin, B. Polsonetti, M.F. Caron, T.F. Oppelt, Infect Dis Ther 13 (1) (2024) 1–19, https://doi.org/10.1007/s40121-023-00900-3.
[11] L. de A.A. Freitas, G. Radis-Baptista, J. Xenobiot. 11(2) (2021) 61–76. 10.3390/jox11020005.
[12] F. Alnahas, P. Yeboah, L. Fliedel, A.Y. Abdin, K. Alhareth, Int. J. Environ. Res. Public Health 17 (2020) 3, https://doi.org/10.3390/ijerph17030787.
[13] M. Sharma, K. Kumar, K.K. Dubey, Environ. Qual. Manag. 30 (4) (2021) 127–140, https://doi.org/10.1002/tqem.21744.
[14] N. Vaszilcsin, A. Kellenberger, M.L. Dan, D.A. Duca, V.L. Ordodi, Materials 16 (2023) 16, https://doi.org/10.3390/ma16165555.
[15] M.N. Nyaga, D.M. Nyagah, A. Njagi, Preprints (Basel) (2020).
[16] N. Vaszilcsin, D. Delia-Andrada, A. Flueraș, M. Dan, Studia Universitatis Babeș-Bolyai Chemia 64 (2019) 17–32. 10.24193/subbchem.2019.3.02.
[17] N.N. Hau, D.Q. Huong, J Mol Struct 1277 (2023) 134884, https://doi.org/10.1016/j.molstruc.2022.134884.
[18] J. Wu, J. Wu, L. Lu, P. Mei, Mater. Chem. Phys. 304 (2023) 127929, https://doi.org/10.1016/j.matchemphys.2023.127929.
[19] K. Tamalmani, H. Husin, Appl. Sci. 10 (10) (2020) 3389, https://doi.org/10.3390/app10103389.
[20] Z.-G. Luo, Y. Zhang, H. Wang, S. Wan, L.-F. Song, B.-K. Liao, X.-P. Guo, Corros Sci 227 (2024) 111705, https://doi.org/10.1016/j.corsci.2023.111705.
[21] A. Rodríguez Torres, M.G. Valladares Cisneros, J. Uruchurtu Chavarín, C. Cuevas Arteaga, M.A. Veloz Rodríguez, Green Chem. Lett. Rev 14(1) (2021) 108–18. Doi: 10.1080/17518253.2020.1862924.
[22] B. Liao, Z. Luo, S. Wan, L. Chen, J. Ind. Eng. Chem. 117 (2023) 238–246, https://doi.org/10.1016/j.jiec.2022.10.010.
[23] T. Gan, Y. Zhang, M. Yang, H. Hu, Z. Feng, D. Chen, C. Chen, J. Liang, Ind. Eng. Chem. Res. 57 (32) (2018) 10786–10797, https://doi.org/10.1021/acs.iecr.8b02128.
[24] J. Haque, M.F.R. Zulkifli, N. Ismail, M.A. Quraishi, M.S. Mohd Ghazali, E. Berdimurodov, W.M.N. Bin Wan Nik, ACS Omega 8(28) (2023) 24797–812. Doi: 10.1021/acsomega.3c00366.
[25] S. Lamghafri, W. Daoudi, O. Dagdag, I.A. Naguib, W. Mohd Norsani Wan Nik, A. Berisha, H. Kim, A. El Aatiaoui, A. Zarrouk, A. Lamhamdi, J. Indust. Eng. Chem. (2024). doi: 10.1016/j.jiec.2024.11.016.
[26] A. Pradityana, F. Khosfirah, F.N. Biwai, R.H.A. Shidieqqy, M.L. Hakim, P.I. Santosa, W.M.N. Wan Nik, Results Eng. 24 (2024) 103037, https://doi.org/10.1016/j.rineng.2024.103037.
[27] R. s Hameed, Portugaliae Electrochim. Acta 29 (2010) 273–85. 10.4152/pea.201104273.
[28] R.S.A. Hameed, S. Obeidat, M.T. Qureshi, S.R. Al-Mhyawi, E.H. Aljuhani, M. Abdallah, J. Mater. Res. Technol. 21 (2022) 2743–2756, https://doi.org/10.1016/j.jmrt.2022.10.081.
[29] M. Abdallah, A. Fawzy, M. Alfakeer, H.M. Altass, Green Chem Lett Rev 14 (3) (2021) 509–518, https://doi.org/10.1080/17518253.2021.1944329.
[30] M. Abdallah, A. Fawzy, A. Al Bahir, Chem. Eng. Commun. 209(2) (2020) 158–70. 10.1080/00986445.2020.1852220.
[31] A.S. Al-Gorair, R. Felaly, N. Fouad, S.S. Al-Juaid, D.F. Seyam, N. Saadan, A.Y. El-Etre, E.M. Mabrouk, M. Abdallah, Green Chem Lett Rev 17 (1) (2024) 2413418, https://doi.org/10.1080/17518253.2024.2413418.
[32] M.G.A. Saleh, M. Alfakeer, R.N. Felaly, M.S. Al-Sharif, S.S. Al-Juaid, K.A. Soliman, M.A. Hegazy, S. Nooh, M. Abdallah, S.A. El Wanees, ACS Omega 9 (27) (2024) 29666–29681, https://doi.org/10.1021/acsomega.4c03135.
[33] R. Abdel-Hameed, M.T. Qureshi, M. Abdallah, E. Aljuhani, A.A. Alzharani, A. Alfarsi, A.M. Bakry, B. Huwaimel, O. Farghaly, Int. J. Electrochem. Sci. 17 (12) (2022) 221270, https://doi.org/10.20964/2022.12.92.
[34] M. Abdallah, K.A. Soliman, M. Alfakeer, H. Hawsawi, A.M. Al-bonayan, S.S. Al-Juaid, S. Abd El Wanees, M.S. Motawea, ACS Omega 8 (38) (2023) 34516–34533, https://doi.org/10.1021/acsomega.3c03257.
[35] M.A. Deyab, O.A.A. El-Shamy, H.K. Thabet, A.M. Ashmawy, Sci. Rep. 13 (1) (2023) 8680, https://doi.org/10.1038/s41598-023-35226-0.
[36] A. Kellenberger, D.A. Duca, M.L. Dan, M. Medeleanu, Materials 15 (8) (2022) 2918.
[37] M. Peng, S. He, C. Wu, Z. Chen, H. Cen, Sustain Chem. Pharm. 36 (2023) 101326, https://doi.org/10.1016/j.scp.2023.101326.
[38] S.C. Nwanonenyi, H.C. Obasi, E.E. Oguzie, I.C. Chukwujike, C.K. Anyiam, J. Bio Tribocorros 3 (4) (2017) 53, https://doi.org/10.1007/s40735-017-0114-z.
[39] A.H. Bakheit, H. Darwish, I.A. Darwish, A.I. Al-Ghusn, in: A. A. Al-Majed (Ed.), Profiles of Drug Substances, Excipients and Related Methodology, Vol. 48, Academic Press, 2023, pp. 71–108.
[40] I. Darwish, N. Khalil, H. Darwish, N. Alzoman, A. Al-Hossaini, J. Mol. Struct. 1263 (2022) 133104, https://doi.org/10.1016/j.molstruc.2022.133104.
[41] K.I. Aly, H.M. Abd El-Lateef, N. Yehia, A. Khodairy, M.M. Sayed, M.A.E.A.A.A. El-Remaily, React. Funct. Polym. 166 (2021) 105001, https://doi.org/10.1016/j.reactfunctpolym.2021.105001.
[42] F. Fotouhiardakani, A. Destrieux, J. Profili, M. Laurent, S. Ravichandran, G. Dorairaju, G. Laroche, Materials 17 (2024) 4, https://doi.org/10.3390/ma17040875.
[43] A.R. Shahmoradi, M. Ranjbarghanei, A.A. Javidparvar, L. Guo, E. Berdimurodov, B. Ramezanzadeh, J. Mol. Liq. 338 (2021) 116550, https://doi.org/10.1016/J.MOLLIQ.2021.116550.
[44] Y. Mehmood, H. Shahid, M. Tahir, M. Abbas, U. Farooq, Z. Khan, H. Youusaf, M. Uddin, M. Kazi, J. Nanopart. Res. 25 (2023), https://doi.org/10.1007/s11051-023-05784-5.
[45] A.M.M. Soliman, K.I. Aly, M.G. Mohamed, A.A. Amer, M.R. Belal, M. Abdel-Hakim, Sci Rep 13 (1) (2023) 5581, https://doi.org/10.1038/s41598-023-30364-x.
[46] M.A. Khan, A.R. Safira, M. Aadil, M. Kaseem, J. Magnesium Alloys 12 (2) (2024) 586–607, https://doi.org/10.1016/j.jma.2023.12.004.
[47] H.M. Abd El-Lateef, M.A.A.A. El-Remaily, A. Khodairy, M.M. Sayed, N. Yehia, M. M. Khalaf, K.I. Aly, J. Mol. Struct 1273 (2023) 134345, https://doi.org/10.1016/j.molstruc.2022.134345.
[48] A.E. Mamaghani, H. Zohoor, K. Firoozbakhsh, R. Hosseini, J. Solid Mechanics 5 (2) (2013) 152–160.
[49] A. Farhadian, S.A. Kashani, A. Rahimi, E.E. Oguzie, A.A. Javidparvar, S. C. Nwanonenyi, S. Yousefzadeh, M.R. Nabid, J. Molecular Liquids 338 (2021) 116607, https://doi.org/10.1016/j.molliq.2021.116607.

[50] Y. Chen, X. Li, Y. Qiang, G. Du, S. Deng, Colloids Surf. A Physicochem. Eng. Asp. 705 (2025) 135555, https://doi.org/10.1016/j.colsurfa.2024.135555.
[51] F. Gebhart, Drug Topics. Http://Drugtopics.Modernmedicine.Com/ Drugtopics/Article/ArticleDetail.Jsp?Id=184115.
[52] A. Ebrahimi-Mamaghani, O. Koochakianfard, N. Mostoufi, H.H. Khodaparast, Appl. Math Model 120 (2023) 330–354, https://doi.org/10.1016/j.apm.2023.03.043.
[53] M. Saket Bejandi, M. Hossein Behroozi, M. Reza Khalili, R. Sharifi, A. Asghar Javidparvar, E. Oguzie, J. Indust. Eng. Chem. 131 (2024) 662–675, https://doi.org/10.1016/j.jiec.2023.11.003.
[54] N. Ellepola, G. Rubasinghege, Environments 9 (7) (2022) 77.
[55] A. Ebrahimi-Mamaghani, O. Koochakianfard, M. Rafiei, A. Alibeigloo, A. Dizaji, V. Borjalilou, Int. J. Struct. Stab. Dyn. (2024), https://doi.org/10.1142/S0219455426500549.
[56] R.A. Pratiwi, A.B.D. Nandiyanto, Indones. J. Educat. Res. Technol. 2 (1) (2021) 1–20.
[57] L. Deng, Y. Xie, G. Zhang, Chin. J. Catal. 38 (2) (2017) 379–388.
[58] A.A. Ramadan, H. Mandil, J. Sabouni, Int. J. Curr. Res. Chem. Pharmaceut. Sci. 7 (8) (2020) 1–15. Doi: 10.22192/ijcrcps.2020.07.08.001.
[59] C. Tang, Z. Chen, A. Farhadian, D. Iravani, C. Chen, Y. Song, A. Rahimi, D. Liang, L. Lu, S. Fan, Energy Fuel 38 (8) (2024) 6738–6752, https://doi.org/10.1021/acs.energyfuels.3c04582.
[60] A. Rahimi, M. Abdouss, A. Farhadian, L. Guo, S. Kaya, J. Neshati, J. Ind. Eng. Chem. 113 (2022) 332–347, https://doi.org/10.1016/j.jiec.2022.06.007.
[61] A. Rahimi, A. Farhadian, L. Guo, E. Akbarinezhad, R. Sharifi, D. Iravani, A. Asghar Javidparvar, M.A. Deyab, M.A. Varfolomeev, J. Ind. Eng. Chem. (2023), https://doi.org/10.1016/j.jiec.2023.03.033.
[62] H. Zhao, S. Deng, Y. Qiang, J. Xu, D. Xu, X. Li, J Mol Liq 407 (2024) 125164, https://doi.org/10.1016/j.molliq.2024.125164.
[63] H.M.K. Sheit, S.M. Kani, M.A. Sathiq, S.S.S. Abuthahir, P. Subhapriya, K. S. Nivedhitha, M.A. Umarfarooq, I.A. Badruddin, S. Kamangar, A.S. Shaik, Materials 17 (2024) 3, https://doi.org/10.3390/ma17030751.
[64] P.H. Renuka, S. Rao, P. Rao, S. Shree S, G.K. Prashanth, Inorg. Chem. Commun. 160 (2024) 111871. doi: 10.1016/j.inoche.2023.111871.
[65] Y. Lv, W. Zhao, Y. Qiang, J. Zhao, Corros Sci 225 (2023) 111601, https://doi.org/10.1016/j.corsci.2023.111601.
[66] R. Farahmand, B. Sohrabi, A. Ghaffarinejad, M.R. Zamani Meymian, Corros. Sci. 136 (2018) 393–401, https://doi.org/10.1016/j.corsci.2018.03.030.
[67] Z. Chen, A. Farhadian, D. Iravani, A. Rahimi, E. Akbarinezhad, C. Chen, Energy Fuel 38 (11) (2024) 9529–9545, https://doi.org/10.1021/acs.energyfuels.4c01684.
[68] M.H. Rahmani, A. Dehghani, M. Salamati, G. Bahlakeh, B. Ramezanzadeh, J. Ind. Eng. Chem. 130 (2024) 368–381, https://doi.org/10.1016/j.jiec.2023.09.040.
[69] S. Mohammadkhah, A. Dehghani, B. Ramezanzadeh, Biomass Convers Biorefin (2023), https://doi.org/10.1007/s13399-023-04163-3.
[70] V.S. Sastri, (1998).
[71] H.-K. Chung, W.-H. Kim, J. Park, J. Cho, T.-Y. Jeong, P.-K. Park, J. Ind. Eng. Chem. 28 (2015) 241–246, https://doi.org/10.1016/j.jiec.2015.02.021.
[72] T. Ishizaki, Y. Masuda, M. Sakamoto, Langmuir 27 (8) (2011) 4780–4788, https://doi.org/10.1021/la2002783.
[73] Z.-H. Huang, X. Zheng, W. Lv, M. Wang, Q.-H. Yang, F. Kang, Langmuir 27 (12) (2011) 7558–7562, https://doi.org/10.1021/la200606r.
[74] A.R. Safira, A. Fattah-alhosseini, M. Kaseem, J. Magnesium Alloys 12 (6) (2024) 2413–2432, https://doi.org/10.1016/j.jma.2024.05.016.
[75] R. Sharifi, A. Ashoori, M. Samanian, A.S. Rouhaghdam, A. Dolati, G.B. Darband, Colloids Surf. A Physicochem. Eng. Asp. 690 (2024) 133687.
[76] S.C. Nwanonenyi, I.O. Arukalam, H.C. Obasi, U.L. Ezeamaku, I.O. Eze, I. C. Chukwujike, M.A. Chidiebere, J. Bio Tribocorros. 3 (4) (2017) 54, https://doi.org/10.1007/s40735-017-0115-y.